Effect of Additive Ti_3SiC_2 Content on Mechanical Properties of $B_4C–TiB_2$ Composites Ceramics Sintered by Spark Plasma Sintering

Xingheng Yan
Science and Technology on Advanced Ceramic Fibers and Composites Laboratory, College of Aerospace Science and Engineering, National University of Defense Technology

Xingui Zhou (17801016168@163.com)
Science and Technology on Advanced Ceramic Fibers and Composites Laboratory, College of Aerospace Science and Engineering, National University of Defense Technology

Honglei Wang
Science and Technology on Advanced Ceramic Fibers and Composites Laboratory, College of Aerospace Science and Engineering, National University of Defense Technology

---

Research Article

Keywords: Spark plasma sintering, Boron carbide, Ti3SiC2, Fracture toughness

Posted Date: September 22nd, 2020

DOI: https://doi.org/10.21203/rs.3.rs-78483/v1

Version of Record: A version of this preprint was published at Materials on October 16th, 2020. See the published version at https://doi.org/10.3390/ma13204616.

Abstract

B_4C-TiB_2 composite ceramics with ultra-high fracture toughness were successfully prepared via spark plasma sintering at 1900℃ using B_4C and Ti_3SiC_2 as raw materials. The results show that compared with pure B_4C ceramics sintered by SPS, the hardness of B_4C-TiB_2 composite ceramics is decreased, but the flexural strength and fracture toughness are significantly improved, especially the fracture toughness has been improved by leaps and bounds. When the content of Ti_3SiC_2 is 30vol.%, the B_4C-TiB_2 composite ceramic has the best comprehensive mechanical properties: hardness, bending strength and fracture toughness are 27.28 GPa, 405.11 MPa and 18.94 MPa·$m^{1/2}$, respectively. The fracture mode of the B_4C-TiB_2 composite ceramics is a mixture of transgranular fracture and intergranular fracture. Two main two reasons for the ultra-high fracture toughness are the existence of lamellar graphite at the grain boundary, and the formation of a three-dimensional interpenetrating network covering the whole composite.

1. Introduction

Boron carbide is an attractive engineering material with a high melting point, low density, high hardness, high thermal conductivity and large neutron absorption surface, which makes it a candidate material for wear-resistant parts, cutting tools, light armor products and neutron radiation shielding[1, 2]. However, the low sintering property (due to the strong B-C covalent bond and B_2O_3 oxide layer) and poor fracture toughness limit its excellent performance. Spark plasma sintering is a kind of electric current assisted sintering technology, which can enhance the bonding and densification of particles through the combination of mechanical pressure, electric field and thermal field[3, 4]. SPS adopts the same stamping/die system concept as hot pressing, and the difference between them is that the heating methods are fundamentally different. Hot pressing sintering is heated by heating body radiation, while the SPS heat source is Joule heat generated by the current of mold or sample[5, 6]. The heating rate of up to 1000 ℃/min can be obtained by SPS, and the heating up time is greatly shortened, which is beneficial to limit the grain growth[7]. In addition, current can also enhance powder sintering by activating one or more parallel mechanisms, such as surface oxide removal, electromigration and electroplasticity[8].

Reasonable use of additives can make boron carbide densification without deterioration of mechanical properties. Some additives can react with boron carbide in situ to form nonvolatile second phases, which is helpful for densification and can enhance properties. Ti_3SiC_2 can react with B_4C to form TiB_2 with high hardness and high melting point, which can be used as an ideal toughening phase for B_4C ceramics[9]. In this study, B_4C-TiB_2 composite ceramics with ultra-high toughness were prepared by the SPS process with different contents of Ti_3SiC_2 as additives, and the influence mechanism of Ti_3SiC_2 content on the microstructure and properties of B_4C-TiB_2 composite ceramics was studied.

2. Experimental Procedure

Commercially available B_4C powders (purity 99.9%, 1 μm, 4.53 g/cm^3, Nangong Naiyate Alloy Welding Material Co., Ltd), Ti_3SiC_2 powders (purity 99.9%, < 74 μm, 4.53 g/cm^3,Nanjing Mingchang New Material Co., Ltd) were used as raw materials. Ti_3SiC_2-B_4C powders containing 20 vol.%, 25 vol.%, 30 vol.% and 35 vol.% Ti_3SiC_2 respectively were mixed for 24 h through a small vertical mixer at 80 r/min without adding solvent. The simples were prepared by SPS equipment (HP D 25/4-SD, FCT Systeme GmbH, Germany) in a vacuum with 35 MPa mechanical pressure at 1900 ℃ for 5 min. The heating rate was 100 ℃/min and the cooling rate was 50 ℃/min.

The absolute density of B_4C-TiB_2 composite ceramics was determined using the Archimedes method. Hardness was measured by a Vickers-indentation tester (Shimadzu, HMV-2TADW E, Japan) at 9.81 N load with a holding time of 15 s on the polished surface. Flexural strength was determined by a three-point bending test with a span of 30 mm and the loading speed of 0.5 mm/min, and the specimens used in the test were 3 × 4 × 35 mm bars. SENB method was used to determine the fracture toughness of the specimens, with dimensions of 2 × 4 × 20 mm (with 2 mm high notch). The microstructures of the composite ceramics were characterized by X-Ray powder diffraction (XRD, X' Pert PRO-MPD, Holland Panalytical, Netherlands), scanning electron microscope (SEM, S-4800N, Hitachi, Japan), transmission electron microscope (TEM, JEM-2100, JEOL, Japan) and energy dispersive spectrometer (EDS, INCA, OXFORD INSTRUMENTS, England).

3. Results And Discussion

The scanning electron microscope (SEM) images and X-ray diffraction (XRD) patterns of the as-received powders of B_4C and Ti_3SiC_2 are shown in Fig. 1. The SEM images show that B_4C particles have ladder-like surface undulation, which is a typical transgranular fracture appearance during the particle crushing process; Ti_3SiC_2 particles have obvious lamellar structure. It can be seen from the XRD images that the two kinds of powders are relatively pure and almost no oxide exists (the content of oxide is too small to be detected in XRD). Figure 2 shows the phase composition of B_4C-TiB_2 ceramic composites prepared at 1900℃ with different content of additive Ti_3SiC_2. There is no diffraction peak of Ti_3SiC_2 in all XRD images, which indicates that Ti_3SiC_2 has completely reacted with B_4C. The overall reaction in the system can be described as the following reaction[10]:

$$3B_4C + 2Ti_3SiC_2 \rightarrow 6TiB_2 + 2SiC + 5C \quad (1)$$

TiC appears as an intermediate product in the whole reaction process but does not exist in the final product. According to the XRD test results, the content of each phase is shown in Table 1. TiB_2 and B_4C are the main phase composition of the composites, and a small amount of SiC and C exist. With the increase of Ti_3SiC_2 content, the proportion of TiB_2, B_4C and C in the composite increases, while the content of B_4C decreases.

Table 1
contents of different phases in B_4C-TiB_2 composite ceramics sintered at different temperatures

Sample name	Content of Ti_3SiC_2 (vol.%)	TiB_2 (wt.%)	B_4C (wt.%)	SiC (wt.%)	C (wt.%)
BT20	20	9.4	87.4	1.6	1.7
BT25	25	19.7	73.2	3.3	3.8
BT30	30	29.6	61.9	4.2	4.4
BT35	35	40.6	47.7	6.1	5.6

Table 2 shows the properties of the samples prepared with different content of Ti_3SiC_2. BT0 is the reference sample without Ti_3SiC_2, and its hardness, bending strength and fracture toughness are 33.5GPa, 224.43 MPa and 5.96MPa·$M^{1/2}$, respectively. Compared with BT0, all samples with Ti_3SiC_2 have higher relative density. Figure 3 shows the BSE images of BT0 and BT30 after polishing. There are some closed pores in BT0, but not in BT30. This is because the B_4C particles have sharp edges and corners, and its hardness (55GPa) is very high. Thus, they can not be extruded and deformed under pressure, leaving a non-contact space inside, and forming pores. The hardness of Ti_3SiC_2 (4GPa) is much smaller than that of B_4C, it can be extruded and deformed without leaving voids between particles under external load. After reaction sintering, TiB_2, B_4C, SiC and C (exist in the form of graphite) in the composites have different thermal expansion coefficients, which make the ceramics more compact after cooling.

Table 2
Properties of ceramics prepared with different content of additive Ti_3SiC_2

Simple name	Content of Ti_3SiC_2 (vol.%)	Density (g/cm^3)	Relative Density (%)	Hardness (GPa)	Flexural Strengh (MPa)	Fracture Toughness ($MPa·m^{1/2}$)
BT0	0	2.50	99.20	33.50	224.43	5.96
BT20	20	3.12	101.16	31.14	317.55	17.68
BT25	25	3.13	101.51	28.70	383.25	18.37
BT30	30	3.17	101.54	27.28	405.11	18.94
BT35	35	3.17	102.28	26.71	343.95	19.00

Because the hardness of the second phase particles produced by the reaction is lower than that of B_4C, especially the graphite phase, it is inevitable that the hardness of the composite ceramics is lower than that of the pure B_4C ceramics. Compared with BT0, the flexural strength and fracture toughness of BT20-

BT35 are improved except for the decrease of hardness. Figure 4 shows the fracture morphology of BT0 and BT30. It can be seen that the fracture surface of BT0 is flat, which is a typical transgranular fracture morphology. While the fracture surface of sample BT30 is rough, which is a typically mixed fracture morphology of transgranular fracture and intergranular fracture. In Fig. 4(b), the dark gray flat area is the B_4C matrix, and the light gray rough area is TiB_2 particles, which indicates that the fracture modes of the B_4C phase and the TiB_2 phase are transgranular fracture and intergranular fracture respectively. In addition, there is a dark gray lamellar phase around the TiB_2 grain, which can be inferred ad graphite phase by energy spectrum analysis. Due to the mismatch of thermal expansion coefficients between B_4C, TiB_2 and graphite (B_4C: $4.5 \times 10^{-6}\ k^{-1}$; TiB_2: $8.1 \times 10^{-6}\ k^{-1}$; Graphite: $1 \times 10^{-6}\ k^{-1}$ in the parallel direction, $29 \times 10^{-6}\ k^{-1}$ in c direction) [11], there will be large residual stress at the interface of the phases, which will induce crack deflection along the grain boundary and extend the crack propagation path to improve the strength and toughness of the material. The nano TiB_2 particles embedded in the B_4C matrix will introduce internal stress, which will strengthen the B_4C matrix by lattice distortion effect, and can also nail the dislocations and hinder their movement, so as to enhance the strength of the material.

It should be noted that the fracture toughness of the composites has a leap forward improvement by adding more than 20vol.% Ti_3SiC_2. The fracture toughness of BT30 is 18.94 $MPa{\cdot}m^{1/2}$, which is more than 3 times of that of BT0 (5.80 $MPa{\cdot}m^{1/2}$) and is more than 2 times higher than the highest fracture toughness cited in Table 3. Wen Q et al[9] adopted the same ratio of raw materials as ours to sinter the ceramics. They used 0.5 μm B_4C powders and 0.5 ~ 10 μm Ti_3SiC_2 powders as raw materials, and their process was 1850 ℃ hot pressing sintering for 30 min. Compared with their work, the particle size of the raw powders we used has more difference in size (B_4C: 1 μm; Ti_3SiC_2: <74 μm), making it easier to form aggregates, which are beneficial for toughness but unfavorable for strength[16]. Besides, our ceramics has a higher relative density and graphite content, which may be due to the evaporation of Si at higher sintering temperature and electric field[17]. Graphite phase exists at the grain boundaries of TiB_2 and B_4C, which reduces the bonding strength of the interface and has an adverse effect on the hardness and strength of the composite ceramics. This is the reason why the flexural strength of BT30 is at a low level in Table 3. But at the same time, the existence of graphite can limit the grain growth. In the cooling process, microcracks are produced under the effect of interfacial stress produced by different thermal expansion coefficients, and the cracks propagate along the interlayer of graphite during fracture, resulting in lamellar pull-out. It can be seen from Fig. 4(b) that there are traces of particle pull-out and lamellar graphite pull-out in the fracture surface of BT30, which is one of the important reasons for the toughening of the composite.

Table 3
Comparison of the properties of the B_4C-TiB_2 composite ceramics reported in recent years

Serial no.	Starting powder	Relative Density (%)	K_{IC}, ($MPa·m^{1/2}$)	Flexural strength (MPa)	Ref. (year)
1	B_4C + 5 wt% (Ti_3SiC_2 + Si)	——	5.61	457.6	[12](2019)
2	B_4C + 30 wt% (TiB_2 + Si)	99.6	5.77	531.2	[13](2018)
3	B_4C + 20 mol%TiB_2	97.9	3.7	——	[14](2020)
4	B_4C + 15 wt%SiC + 20 mol%TiB_2	98.6	4.2	343.8	[15](2020)
5	B_4C + 6.45vol.%SiC + 7.78vol.%TiB_2	99.62	6.38	632	[16](2019)
6	B_4C + 30vol.% Ti_3SiC_2	98.72	8.0	492.3	[9](2017)
BT30	B_4C + 30vol.% Ti_3SiC_2	101.54	18.94	405.11	This work

Figure 5 shows the variation of relative density and hardness of B_4C-TiB_2 composite ceramics with the content of Ti_3SiC_2. Due to the slight evaporation of silicon[17], the density of composites is slightly higher than the theoretical density. The evaporation capacity of Si increases with the increase of Ti_3SiC_2 content, resulting in an increase of the relative density. The hardness decreases with the increase of Ti_3SiC_2 content because of the proportion of the second phase with lower hardness, especially graphite, increases.

Figure 6 shows the variation of flexural strength and fracture toughness of B_4C-TiB_2 composite ceramics with additive Ti_3SiC_2 content. When the content of Ti_3SiC_2 is in the range of 20vol.% ~ 30vol.%, the flexural strength and fracture toughness are positively correlated with the content of Ti_3SiC_2. Compared Fig. 7(a)-(c), it can be seen that the region as shown in Fig. 7(e) becomes larger and more numerous with the increase of Ti_3SiC_2 content. In this region, TiB_2, graphite and B_4C intersect each other to form a three-dimensional interpenetrating network. During the crack propagation process, multiple two-phase interfaces must be bypassed to disperse into more small cracks and a large number of changes in the propagation direction. The pull-out mechanism of graphite also plays an important role in this agglomeration area. Besides, this area does not exist in isolation. Every small network links to each other, forming a large network structure covering the whole composite. At the same time, the network divides the B_4C concentration area into small parts and surrounds them, so that there is no large area of continuous B_4C phase in the composites, which is very unfavorable to the toughness of the composite.

With the increase of interlacing degree of TiB_2, graphite and B_4C, the cracks need to bypass more two-phase interfaces, change more directions and disperse into more small cracks. Therefore, the fracture toughness of B_4C-TiB_2 composite ceramics is greatly improved by the overall three-dimensional interpenetrating network structure.

However, when the content of Ti_3SiC_2 is 35 vol.%, as shown in Fig. 6 (d), a large TiB_2-SiC agglomerated area appears in the BT35 (among which the dark gray, medium gray and light gray phases are B_4C, SiC and TiB_2 respectively). There is a bad stress effect in the multiphase mixing region with more SiC. At higher magnification Fig. 7(f), many microcracks due to mismatch of thermal expansion coefficient can be found in this region, which is conducive to the toughening of the material. Nevertheless, it has a bad effect on the bending strength, resulting in a significant decrease in the bending strength.

4. Conclusions

Ultra-high toughness B_4C-TiB_2 composite ceramics were prepared by the SPS method at 1900℃. The content of additive Ti_3SiC_2 has a great influence on the microstructure and mechanical properties. With the increase of Ti_3SiC_2 content, the relative density and fracture toughness of the material increase, while the hardness decreases, and the flexural strength first increases and then decreases. When the content of Ti_3SiC_2 is 30 vol.%, B_4C-TiB_2 composite ceramics have the highest bending strength and the best comprehensive mechanical properties: hardness 27.28 GPa, bending strength 405.11 MPa, fracture toughness 18.94 $MPa{\cdot}m^{1/2}$. The fracture mode of the material is a mixture of transgranular fracture and intergranular fracture. The main reason for obtaining high fracture toughness is the existence of the graphite phase and the formation of a three-dimensional interpenetrating network covering the whole composite. The existence of the graphite phase has an effect on the hardness and fracture toughness of B_4C-TiB_2 composite ceramics, but they still remain at a high level.

References

1. Suri AK, Subramanian C, Sonber JK, et al. Synthesis and consolidation of boron carbide: a review. International Materials Reviews 2013; 55(1):4-40.
2. Domnich, Vladislav, Reynaud, et al. Boron Carbide: Structure, Properties, and Stability under Stress. 2011; 94(11):3605-3628.
3. Ghosh S, Chokshi AH, Lee P, et al. A Huge Effect of Weak dc Electrical Fields on Grain Growth in Zirconia. 92(8):1856-1859.
4. Zhang ZH, Liu ZF, Lu JF, et al. The sintering mechanism in spark plasma sintering – Proof of the occurrence of spark discharge. 81:56-59.
5. Langer J, Hoffmann MJ, Guillon OJAM. Direct comparison between hot pressing and electric field-assisted sintering of submicron alumina. 57(18):5454-5465.

6. Langer J, Hoffmann MJ, Guillon O. Electric Field-Assisted Sintering in Comparison with the Hot Pressing of Yttria-Stabilized Zirconia. Journal of the American Ceramic Society 2011; 94(1):131-138.
7. Munir ZA, Anselmi-Tamburini U, Ohyanagi M. The effect of electric field and pressure on the synthesis and consolidation of materials: A review of the spark plasma sintering method. Journal of Materials Science 2006; 41(3):763-777.
8. Gao H, Asel TJ, Cox JW, et al. Native point defect formation in flash sintered ZnO studied by depth-resolved cathodoluminescence spectroscopy. 120(10):105302.
9. Wen Q, Tan Y, Zhong Z, et al. High toughness and electrical discharge machinable B4C-TiB2-SiC composites fabricated at low sintering temperature. Materials Science and Engineering: A 2017; 701:338-343.
10. He P, Dong S, Kan Y, et al. Microstructure and mechanical properties of B4C–TiB2 composites prepared by reaction hot pressing using Ti3SiC2 as additive. Ceramics International 2016; 42(1):650-656.
11. Zhang X, Zhang Z, Wang W, et al. Preparation of B4C composites toughened by TiB2-SiC agglomerates. 2016:S0955221916304824.
12. Song Q, Zhang Z-H, Hua Z-Y, et al. Microstructure and mechanical properties of super-hard B4C ceramic fabricated by spark plasma sintering with (T3SiC2+Si) as sintering aid. Ceramics International 2019; 45(7):8790-8797.
13. Yin S-P, Zhang Z-H, Cheng X-W, et al. Spark plasma sintering of B4C-TiB2-SiC composite ceramics using B4C, Ti3SiC2 and Si as starting materials. Ceramics International 2018; 44(17):21626-21632.
14. Liu Y, Wu X, Liu M, Huang Y, et al. Microstructure and mechanical properties of B4C–TiB2–SiC composites fabricated by spark plasma sintering. Ceramics International 2020; 46(3):3793-3800.
15. Liu Y, Li Z, Peng Y, et al. Effect of sintering temperature and TiB2 content on the grain size of B4C-TiB2 composites. Materials Today Communications 2020; 23.
16. Zhang X, Zhang Z, Liu Y, et al. High-performance B4C–TiB2–SiC composites with tuneable properties fabricated by reactive hot pressing. Journal of the European Ceramic Society 2019; 39(10):2995-3002.
17. Zhang Z, Xu C, Du X, et al. Synthesis mechanism and mechanical properties of TiB2–SiC composites fabricated with the B4C–TiC–Si system by reactive hot pressing. Journal of Alloys and Compounds 2015; 619:26-30.

Figures

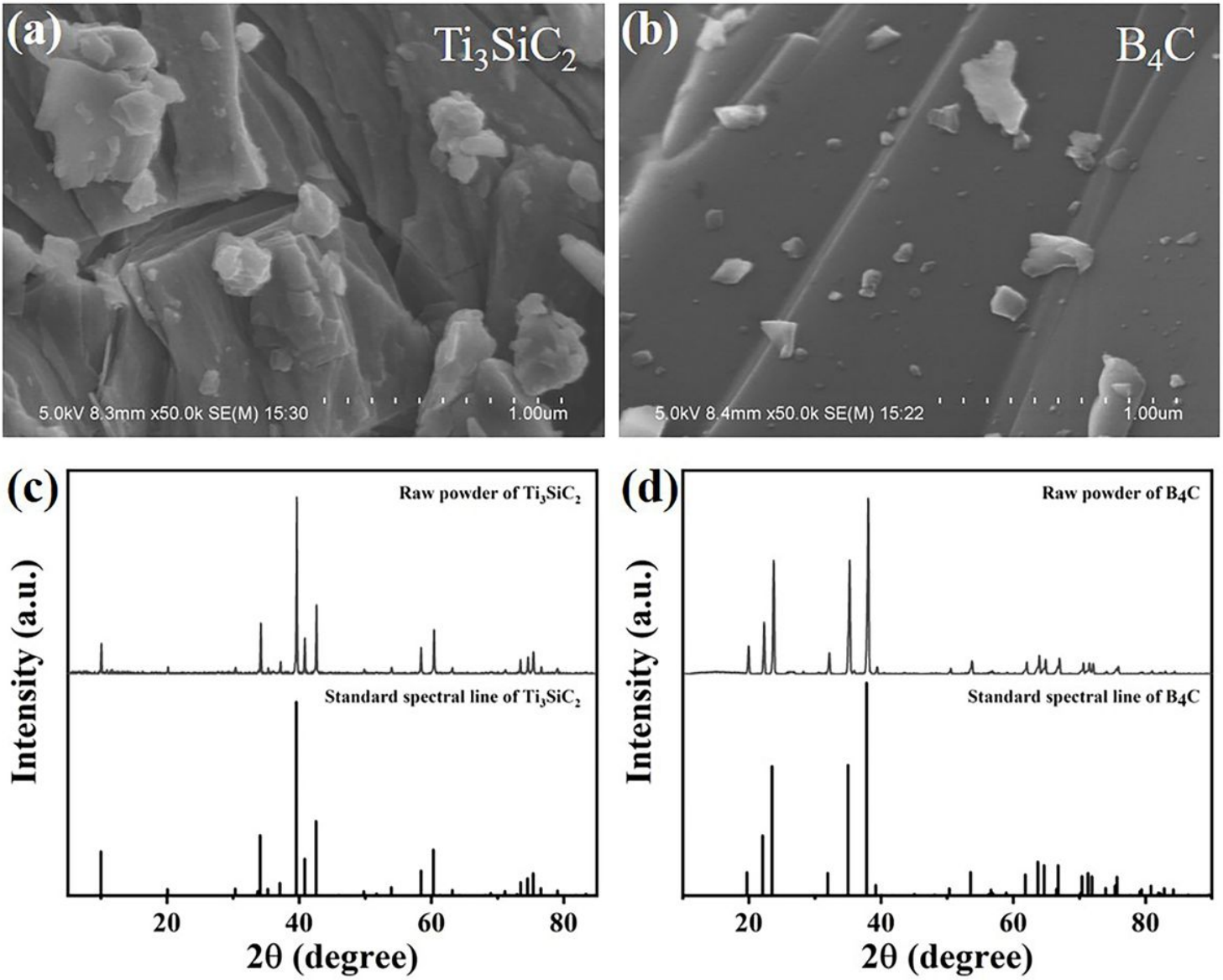

Figure 1

SEM images and XRD patterns of raw powders

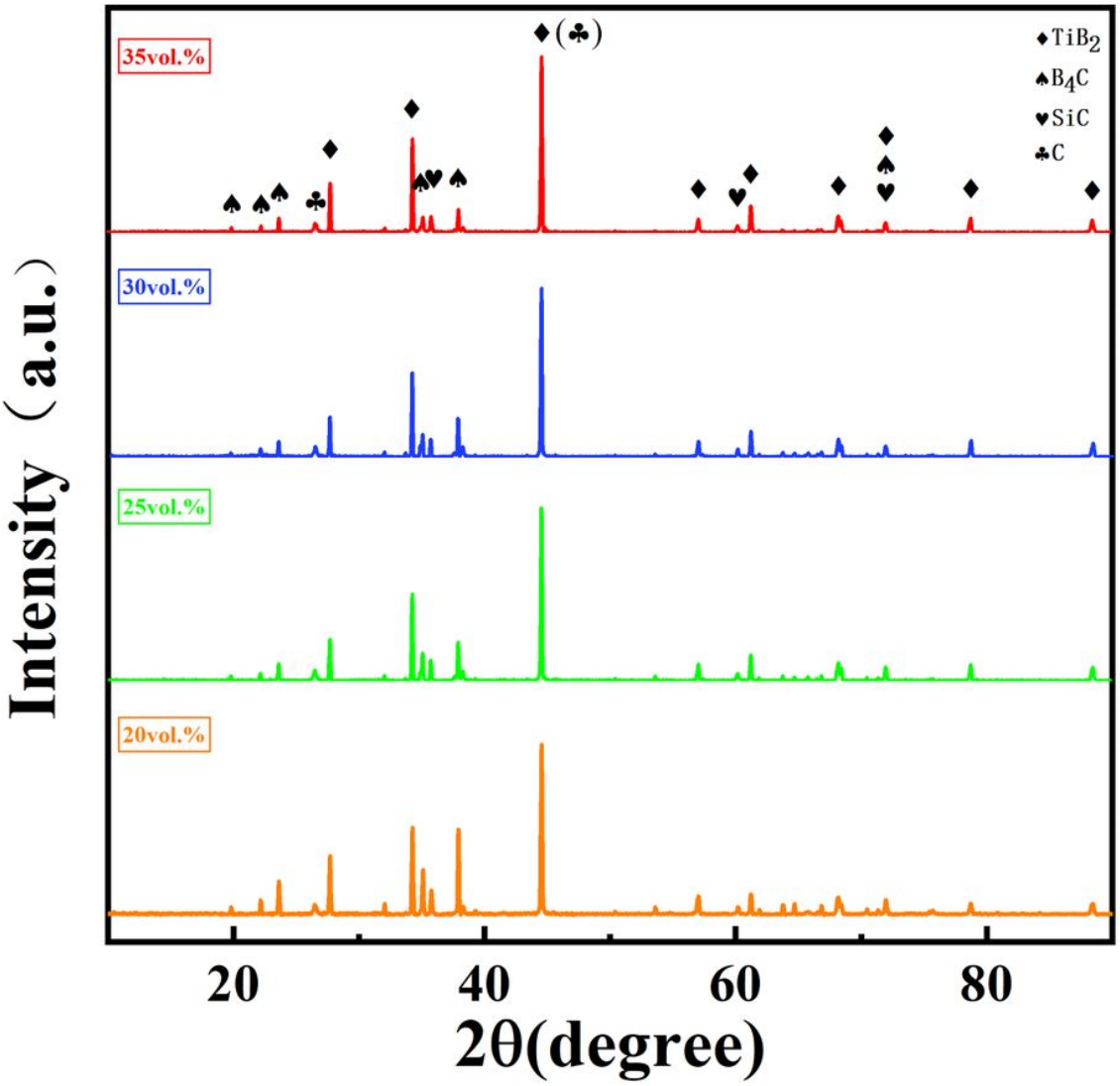

Figure 2

XRD patterns of B4C-TiB2 ceramic composites sintered at 1900°C with different content of additive Ti3SiC2

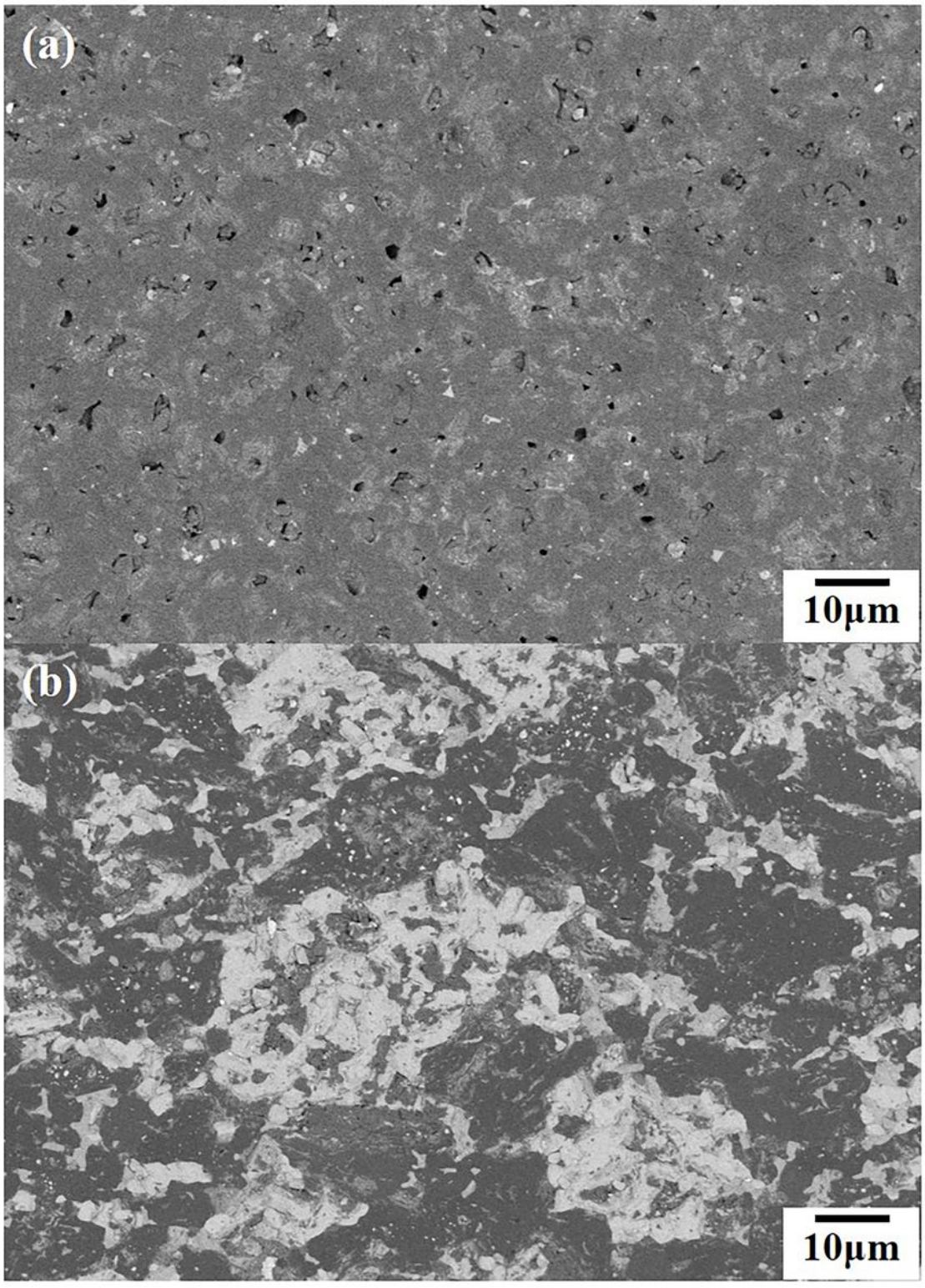

Figure 3

(a) BSE image of BT0; (b) BSE image of BT30

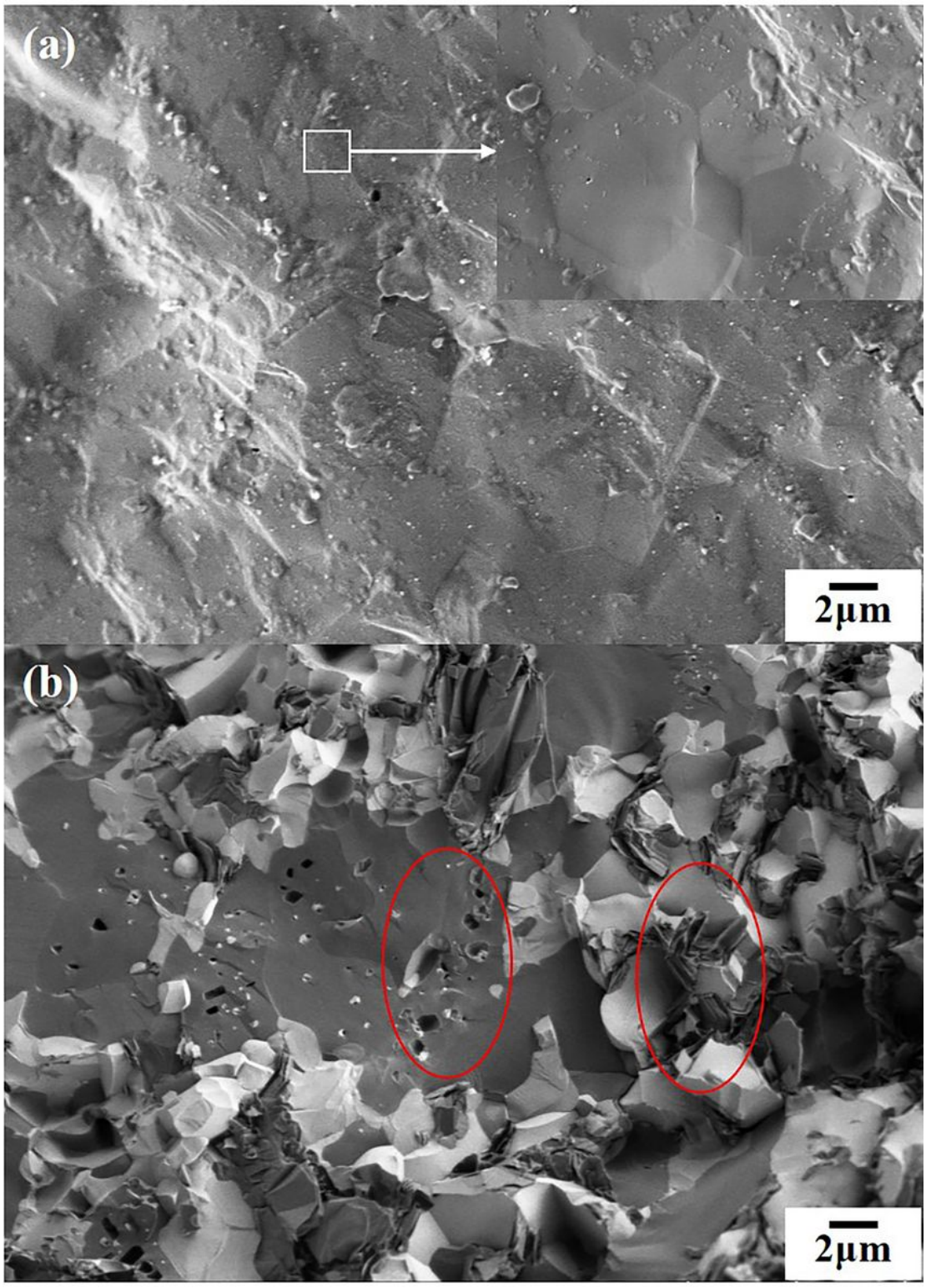

Figure 4

(a) SEM image of fracture surface of BT0; (b) SEM image of fracture surface of BT30

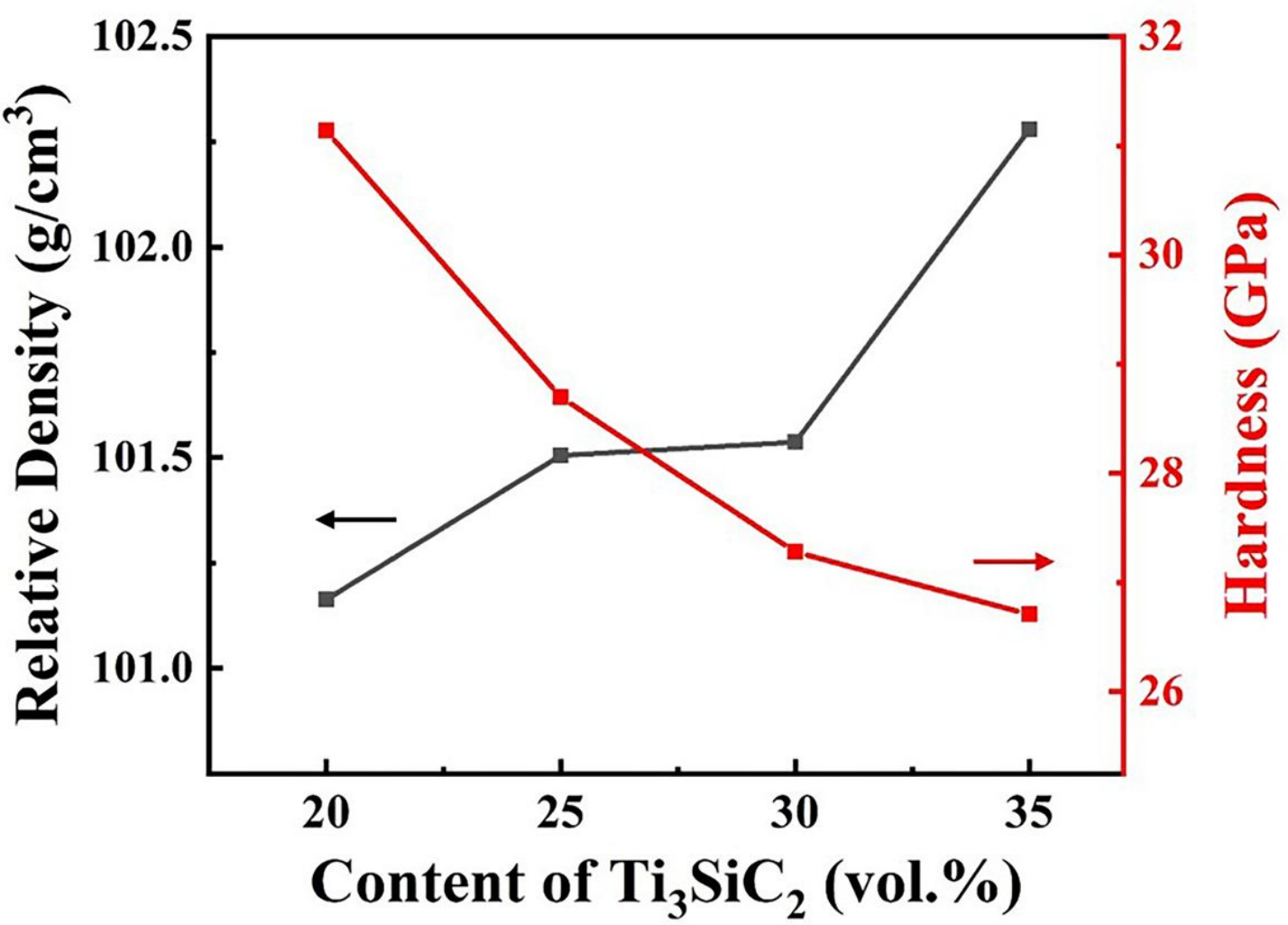

Figure 5

Relative density and hardness of the B4C-TiB2 composite ceramics sintered with different content of Ti3SiC2

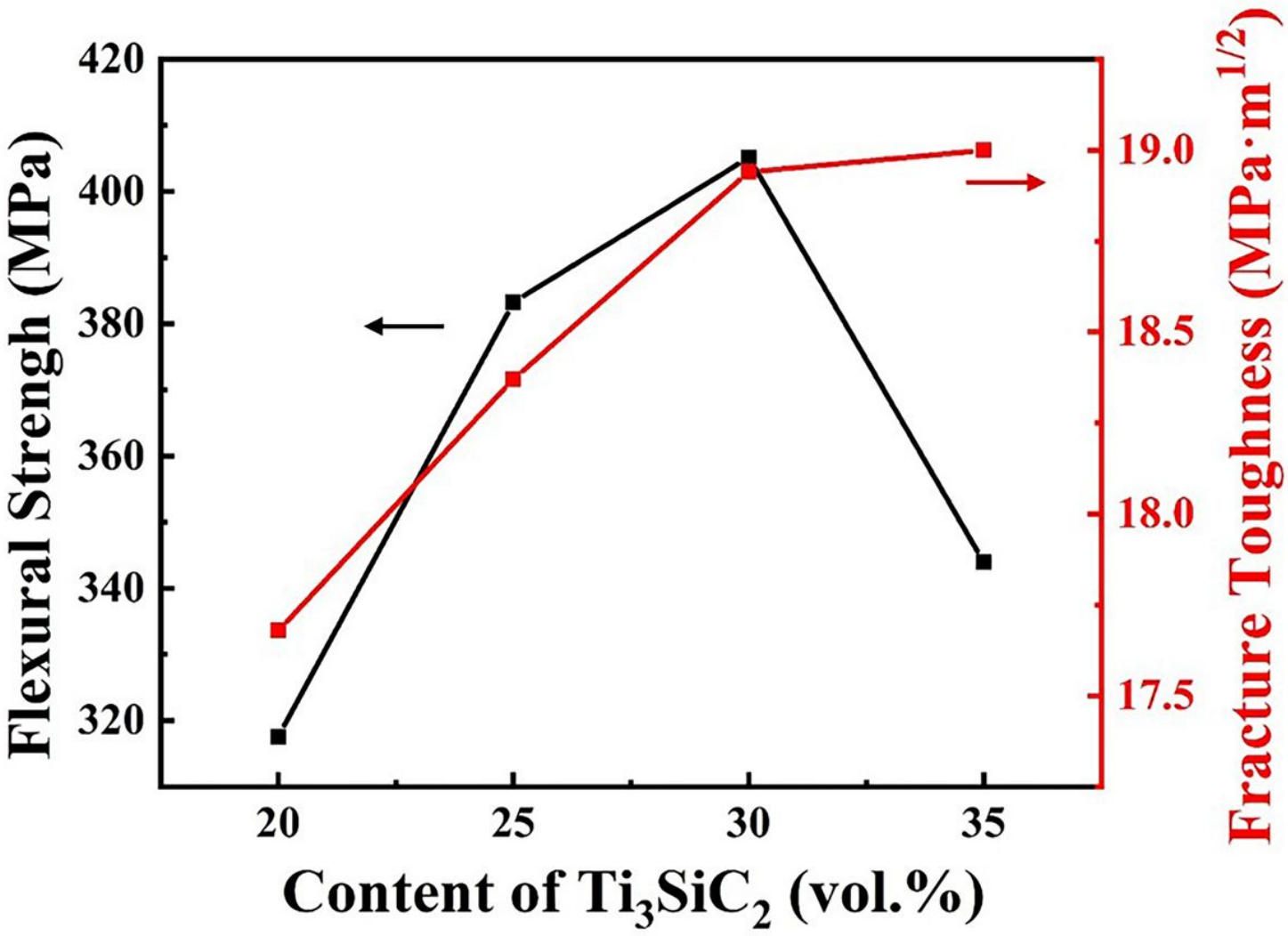

Figure 6

Flexural strength and fracture toughness of the B4C-TiB2 composite ceramics sintered with different content of Ti3SiC2

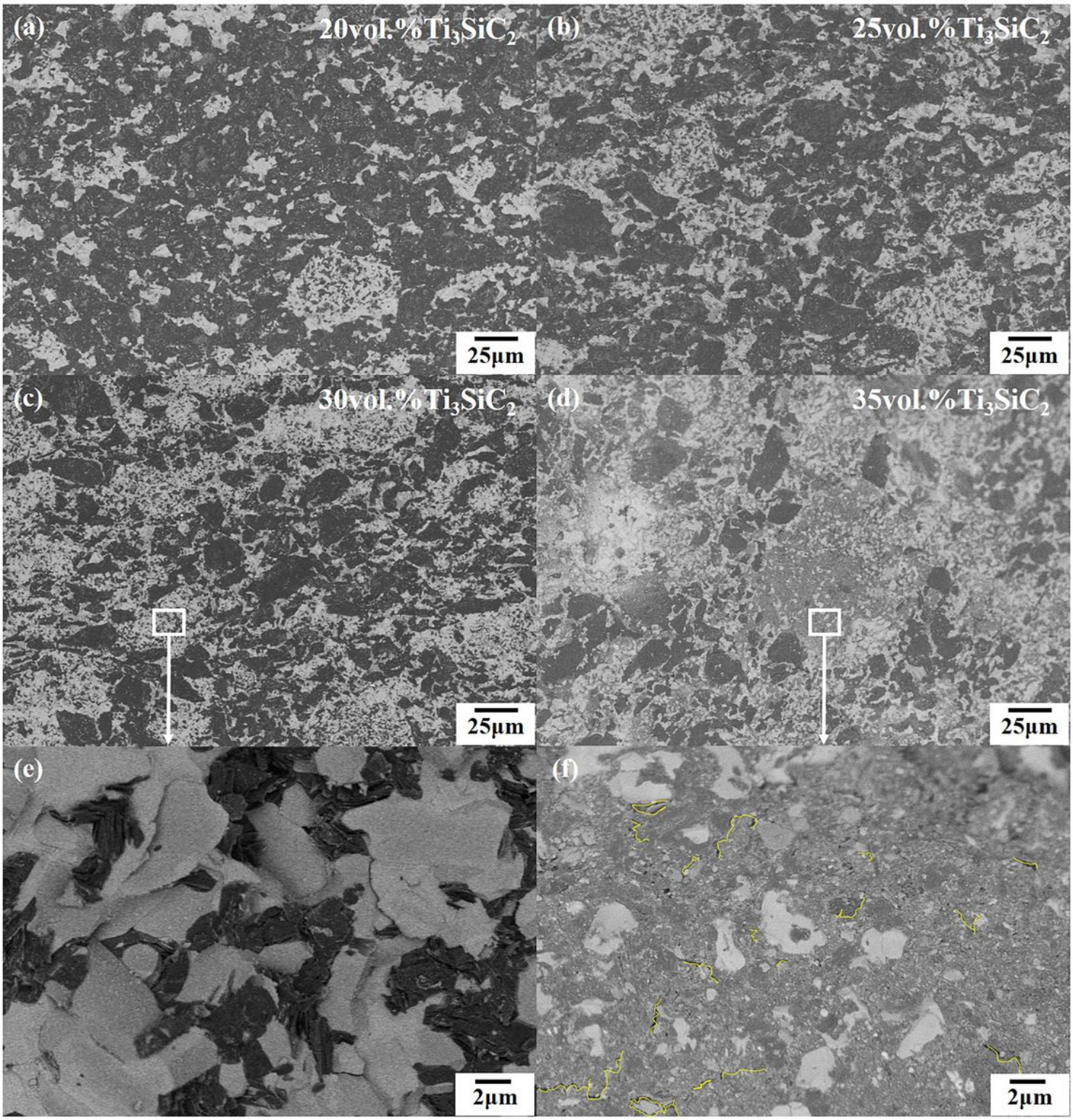

Figure 7

BSE images of B4C-TiB2 composite ceramics sintered with different content of Ti3SiC2